AGU PUBLICATIONS

Geophysical Research Letters

RESEARCH LETTER
10.1002/2016GL072228

Key Points:
- We clarify the complex rupture process for the 2016 Kaikoura earthquake by using a combined analysis of optical satellite and seismology data
- The Kaikoura earthquake involved major coseismic slip on several previously unknown faults
- Simultaneous coseismic slip occurred on the Kekerengu Fault (strike-slip) and a deeper shallow-dipping fault (oblique-slip)

Supporting Information:
- Supporting Information S1
- Movie S1
- Figure S1
- Figure S2

Correspondence to:
J. Hollingsworth,
james.hollingsworth@univ-grenoble-alpes.fr

Citation:
Hollingsworth, J., L. Ye, and J.-P. Avouac (2017), Dynamically triggered slip on a splay fault in the M_w 7.8, 2016 Kaikoura (New Zealand) earthquake, *Geophys. Res. Lett.*, *44*, 3517–3525, doi:10.1002/2016GL072228.

Received 6 DEC 2016
Accepted 13 MAR 2017
Accepted article online 20 MAR 2017
Published online 21 APR 2017

Dynamically triggered slip on a splay fault in the M_w 7.8, 2016 Kaikoura (New Zealand) earthquake

James Hollingsworth[1,2], Lingling Ye[3], and Jean-Philippe Avouac[3]

[1]Université Grenoble Alpes, ISTerre, Grenoble, France, [2]CNRS, ISTerre, Grenoble, France, [3]Seismological Laboratory, California Institute of Technology, Pasadena, California, USA

Abstract We investigate the M_w 7.8, 2016 Kaikoura (New Zealand) earthquake by using optical satellite imagery and seismology to reveal the main features of the rupture process. Correlation of Landsat8 images reveals a 30–40 km surface rupture on the Kekerengu Fault and Jordan Thrust, with up to 12 m of right-lateral slip. A previously unrecognized conjugate strike-slip fault, the Papatea Fault, also slipped coseismically (3–4 m). The global centroid moment tensor (gCMT) centroid indicates both thrust and right-lateral slip and is located ~100 km NE of the main shock epicenter. The significant non-double-couple component of the gCMT (25%) suggests that the main shock is not well represented by a single planar fault. Back projection of teleseismic *P* waves reveals two main bursts of seismic radiation: (1) at 10–20 s, near the main shock epicenter, and (2) at ~70 s, close to the observed surface ruptures. We determine a finite source kinematic model of the rupture from the inversion of seismic waveforms. We use two faults in our model, defined to match the observed slip on the Kekerengu Fault, and a deeper offshore fault with a lower dip angle to satisfy the long period seismological observations. We compute the equivalent moment tensor from our finite source model and find it to be remarkably consistent with the gCMT solution. Although little is known about the geometry of these faults at depth, if the Kekerengu Fault splays from the deeper thrust, then it provides a rare example where the contribution of slip on a splay fault can be clearly isolated in the seismological waveforms.

Plain Language Summary Through a combined analysis of satellite images and seismic waves, we investigate the recent M_w 7.8 earthquake near Kaikoura, New Zealand. We observe major surface ruptures, with up to 12 m strike-slip displacement, located far from onset of earthquake slip. Properties of the seismic waves indicate that the earthquake slipped on a dipping thrust fault at depth and propagated to the northeast for 120 s. Halfway through the rupture, the earthquake triggered simultaneous slip on a neighboring fault, which possibly splays from the main thrust, and which was responsible for the observed surface offsets. Splay faults are commonly observed at converging plate boundaries globally and are suspected to pose a seismic and tsunamic hazard. This is the first time where simultaneous slip on a possible megathrust and associated splay fault has been directly observed in the seismic data.

1. Introduction

On 13 November 2016, a large magnitude (M_w 7.8) earthquake struck the north-east coast of South Island New Zealand, in a zone of oblique convergence between the Pacific and Australian plates (Figure 1). The epicenter reported by the U.S. Geological Survey (USGS) was located in the Marlborough region of South Island, 60 km southwest of Kaikoura, close to where the Waiau River cuts across the Lowry Peaks Range (Figure 1). The earthquake is the largest to have occurred in the Marlborough region for 168 years, since the 1848 Blenheim (M_w 7.5) earthquake, which broke the eastern section of the Awatere Fault [*Mason and Little*, 2006, Figure 1]. The long period seismic waves indicate a source mechanism, represented by the global centroid moment tensor (gCMT) solution (www.globalcmt.org/), with about equal thrust slip and right-lateral strike slip on a NE-SW fault dipping 33° to the northwest (Figure 1). The W-phase solution is not very stable due to the moderate size of the earthquake and probable complexity of the source but yields nodal planes consistent with the gCMT solution (strike: 219, dip: 38, rake: 128, see http://earthquake.usgs.gov/earthquakes/eventpage/us1000778i#executive). The slip vector is approximately parallel to the convergence across the Marlborough Fault System. The strike is consistent with known geological structures across the region, but the dip angle is significantly shallower than the dip angles near the surface [*Litchfield et al.*, 2014] (Figure 1). The significant non-double-couple component of the gCMT (25%, defined in the New Manual of

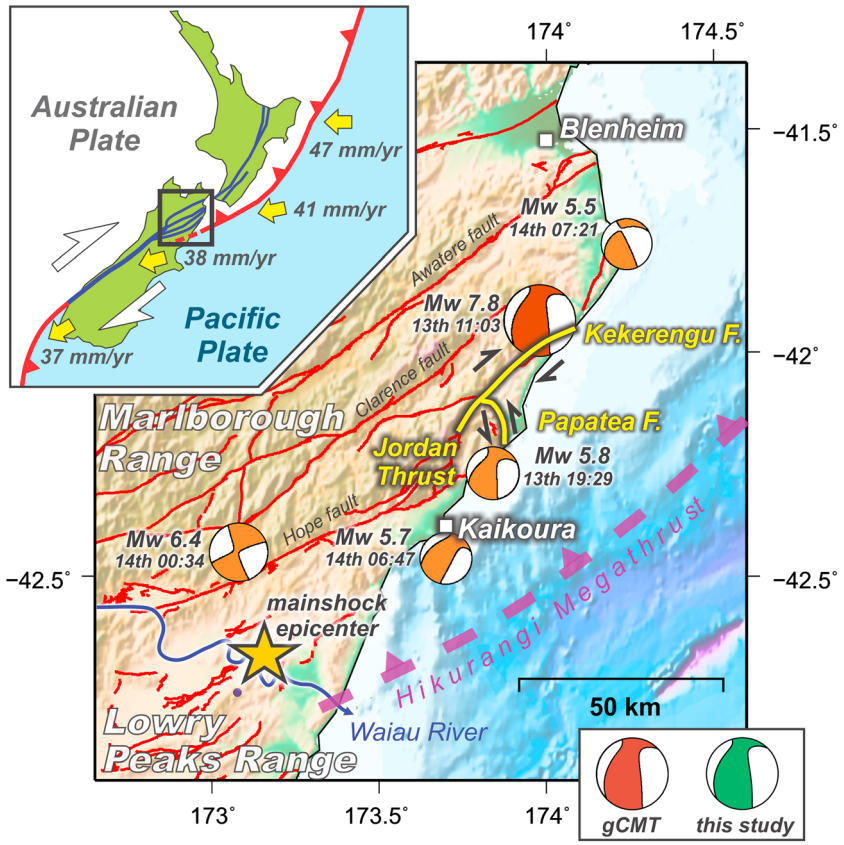

Figure 1. Topographic map showing the Marlborough region of South Island New Zealand affected by the 2016 Kaikoura earthquake. The blue line shows the Waiau River. The red lines show faults from the New Zealand Active Faults Database (GNS Science, https://data.gns.cri.nz/af). The purple dashed line shows the approximate western extent of the Hikurangi Megathrust. The yellow lines show locations of surface ruptures on the Kekerengu and Papatea Faults activated during the main shock event (this study). The yellow star shows the location of the main shock epicenter as determined by the USGS. Global CMT fault plane solutions are shown in orange (at centroid locations); the main shock is shown in dark orange. The lower right inset compares the gCMT main shock solution (dark orange) with our best fit source model (green). Tectonic setting of New Zealand is given in the upper left inset; the black box shows the Marlborough region.

Seismological Observatory Practice [*Bormann et al.*, 2009]) and of the W-phase solution (43%) suggests that the main shock is not well represented by a single point source and probably involved rupture of several faults with different seismic radiation patterns. Field observations do indeed suggest a complicated surface faulting pattern (such as http://info.geonet.org.nz/pages/viewpage.action?pageId=20971550). In this study we document surface deformation by using optical satellite images and combine this with teleseismic observation to reveal the first-order features of the Kaikoura earthquake rupture process.

2. Optical Satellite Geodesy

Correlation of optical satellite images can provide information on the near-field surface displacement field produced by an earthquake [e.g., *Avouac and Leprince*, 2015]. Regular global acquisitions of optical satellite imagery from a variety of sensors (e.g., Landsat8) provide a rich archive of data from which we can narrowly isolate a time period spanning an earthquake. Landsat8 images covering the northeastern section of the epicentral area were first acquired on 13 November (11 h after the main shock). Despite heavy cloud coverage in these first post-earthquake images, much of the coastline northeast of Kaikoura was cloud-free. Later cloud-free images covering the entire epicentral region were acquired on 15 December 2016. We correlate post-earthquake Landsat8 images from 15 December 2016 with cloud-free pre-earthquake images acquired on 13 December 2015. The similar season of the two image acquisitions results in the same

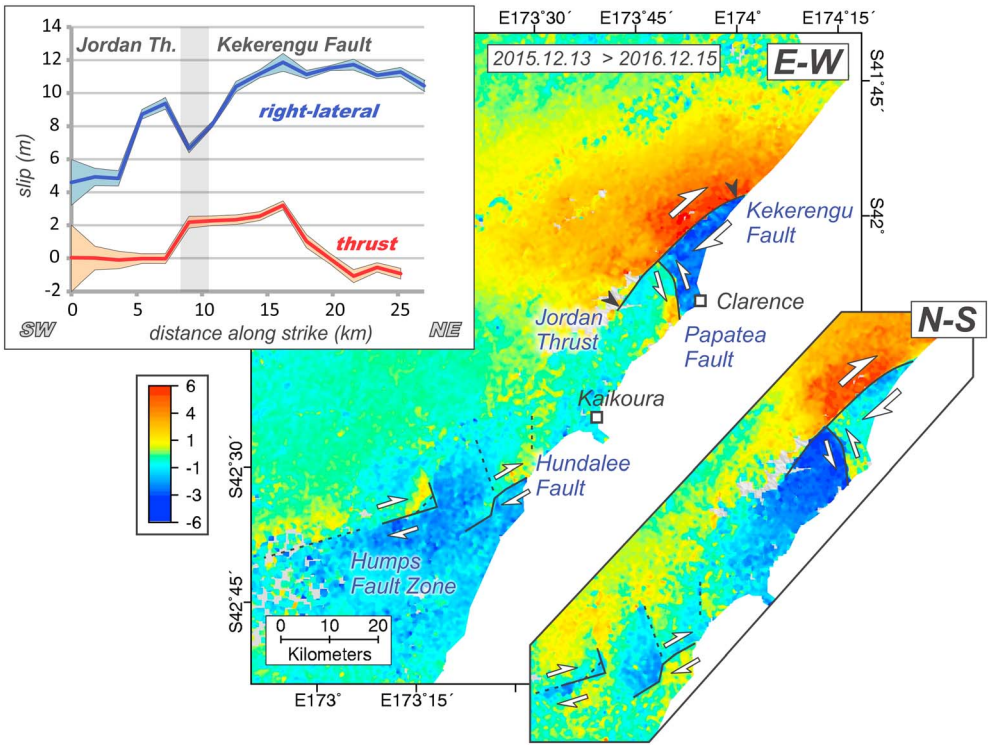

Figure 2. East-west horizontal displacement field for the Kaikoura region computed by using optical image correlation of Landsat8 satellite images. A multiscale correlation window (64–32 pixels) was used, with a step-size of 4 pixels. The data were filtered by using a 5 × 5 median filter. The black lines show surface ruptures associated with the Kekerengu Fault, Jordan Thrust, Papatea Fault, Hundalee Fault, and Humps Fault Zone. The lower right inset shows the north-south displacement field. The red values indicate east/north movement; the blue value is west/south (green is stable). The upper left inset shows the along-strike displacement values (strike slip and thrust) extracted from a series of swath profiles across the Jordan Thrust and Kekerengu Faults (between black pointers). The error bars represent the standard deviation in the linear regressions used to measure the offset [see *Ayoub et al.*, 2015]; the low apparent error is a function of the smoothing applied.

Sun illumination properties in each image, thereby reducing the effect of shadow differences biasing the correlator and producing topographically correlated noise. In addition, minor vegetation cover, agriculture, or urbanization across the region all contribute to the excellent correlation characteristics (Figure 2). We also correlate the pre-earthquake image (13 December 2015) with the first post-earthquake images (13 November 2016) and subtract this from our 15 December 2016 correlation (Figure 2), to check we are not sensitive to additional shallow postseismic slip occurring within the first 2 months (Figure S1 in the supporting information). We find no significant displacements between 13 November and 15 December 2016, suggesting that any postseismic deformation is below the detection level of Landsat8 correlation (typically ~1 m).

Landast8 images were obtained from the USGS EarthExplorer website (http://earthexplorer. usgs.gov/) and correlated by using the COSI-Corr software package (COSI-Corr, available for free download from www.tectonics.caltech.edu/slip_history/spot_coseis/ index.html) [*Leprince et al.*, 2007; *Ayoub et al.*, 2015]. Subpixel precision is achieved by measuring the phase shift of the low-frequency content between both images by using a sliding window [*Leprince et al.*, 2007]. Therefore, despite the images being only 15 m resolution, we can resolve down to ~1 m ground displacements for each window [e.g., *Avouac et al.*, 2014; *Zinke et al.*, 2014]. The technique yields an independent displacement measurement every 480 m for a 32 pixel correlation window size. To reduce noise in the correlation results, we discard extreme outliers, remove a linear trend, and apply a 5 × 5 median filter. Because the Landsat8 sensor is nadir-looking, differences between the two images correspond to purely horizontal deformation (this viewing geometry also helps to reduce topographically correlated noise, which occurs due to the stereo effect between oblique-view images [e.g., *Copley et al.*, 2011; *Hollingsworth et al.*, 2012]).

The region covering the main shock epicenter, as indicated by aftershocks, correlates well; the EW and NS displacement fields are shown in Figure 2. A striking feature of the correlation is a clear surface rupture on the Kekerengu Fault and Jordan Thrust, spanning a distance of ~35 km, before continuing offshore to the northeast. Displacement is predominantly right-lateral strike slip (up to 12 m), with a small thrust component (1–2 m, see Figure 2, upper left inset). The horizontal slip vector is everywhere approximately parallel to the fault trace indicating a dominantly strike-slip motion along the curved geometry of the fault. The asymmetry of surface deformation suggests a rather steep dip angle consistent with values of 70° to 90° reported from previous geological field investigations [*Knuepfer*, 1992; *Litchfield et al.*, 2014, and references therein].

A previously unmapped conjugate fault, the Papatea Fault (http://info.geonet.org.nz/display/quake/2016/11/16/Ruptured+land%3A+observations+from+the+air), intersects the Kekerengu Fault ~20 km NW of the town of Clarence and slipped by ~4 m (left-lateral) and ~3 m (thrust), before striking to the south and continuing offshore (Figure S2, lower left inset).

Southwest of the intersection between the Kekerengu Fault and the Papatea Fault, slip continues on the Jordan Thrust (right-lateral strike slip) before dying out at the intersection with the Hope Fault, which is a well-known active structure accommodating much of the regional shear across the Marlborough Fault System [*Van Dissen and Yeats*, 1991; *Litchfield et al.*, 2014]. No substantial surface slip is resolvable southwest of the Jordan Thrust for 40 km, at which point several smaller surface ruptures are seen on different faults within the main shock epicentral region, including the Hundalee Fault, and Humps Fault Zone (Figure S2). A large right-lateral aftershock (M_w 6.4) on 14 November (~12 h after the main shock) is consistent with the location and slip-style of the Humps Fault Zone rupture (Figure S2). However, due to a lack of available cloud-free imagery before this aftershock, it is unclear if this fault broke in the main shock or in the aftershock.

The discontinuous nature of surface ruptures in the southwest, coupled with lower slip values and shorter rupture lengths, is in sharp contrast with the Kekerengu Fault to the northeast. Therefore, our measurements suggest that no significant continuous surface rupture occurred during the main shock in the epicentral area, which extends far beyond the southwest limit of the Kekerengu Fault (Figure 1).

3. Seismological Constraints

We image the rupture process by back-projecting teleseismic *P* waves recorded by the large aperture Australian seismic network [*Ishii et al.*, 2005]. Broadband teleseismic *P* waves are aligned on reference arrival times of the IASP91 model from USGS/National Earthquake Information Center (NEIC) hypocenter by multi-station cross correlation and separately back-projected to a horizontal surface around the source region following the procedure of *Xu et al.* [2009]. We band-pass filtered the seismograms between 0.5 and 2 Hz (Figure 3). Coherent high-frequency seismic radiation is imaged during 120 s from the onset of the rupture. The animation (Movie S3 in the supporting information) shows a northeastward unilateral rupture. We observed two main bursts of seismic radiation. The first one, between 10 s and 20 s, occurred close to the main shock epicenter. The inferred rupture speed is 2.0–2.5 km/s. The second one, at ~70 s, occurred close to the centroid and the main surface rupture imaged from optical image correlation (Figure 2). The two sources are separated by ~90 km in map view and ~60 s in time, suggesting a rather slow rupture propagation of ~1.5 km/s, or two distinct subevents. The northeastward propagation revealed by this analysis is consistent with the gCMT centroid location lying 118 km northeast of the epicenter.

We next determined a finite source kinematic model of the rupture from the inversion of the seismic waveforms in the 0.005–0.9 Hz frequency band, using a least squares procedure with a specified fault-model geometry and rupture expansion speed [e.g., *Hartzell and Heaton*, 1983; *Ye et al.*, 2016]. We first tested models involving only one planar fault by using the best double-couple fault geometry from the gCMT moment tensor solution (Figure S4). This source model is close to the USGS finite source solution (http://earthquake.usgs.gov/earthquakes/eventpage/us1000778i#finite-fault), although our model is smoother due to using a slightly shallower-dipping fault plane (33° versus 38°). The model is consistent with the coastal uplift reported by GNS (http://info.geonet.org.nz/pages/viewpage.action?pageId=20971591) and the tsunami excitation (http://www.linz.govt.nz/sea/tides/sea-level-data/sea-level-data-downloads) but is inconsistent with the surface faulting reported here or from field mapping [*Litchfield et al.*, 2016]. A fault geometry with a single fault more consistent with the surface ruptures along the Kekerengu and Jordan Faults would not allow us to

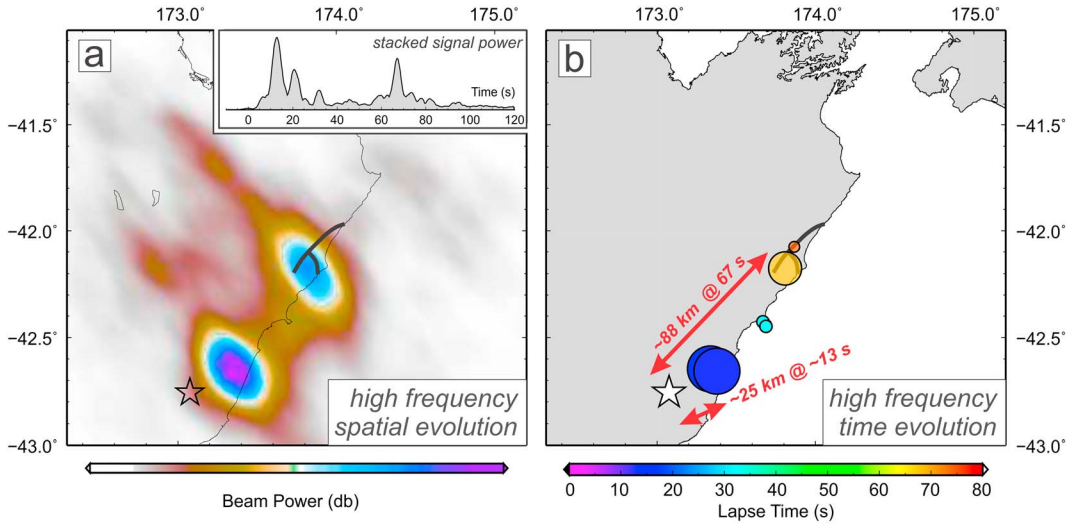

Figure 3. (a) Spatial distribution of time-integrated beam power for 0.5–2.0 Hz *P* wave back projections from the Australia networks. The star indicates the main shock epicenter. The black lines show the Kekerengu and Papatea Faults. The top right inset shows the stacked signal power as a function of time. (b) Elapsed time color-coded local maxima of time-integrated images, indicating the foci of coherent high-frequency radiation. The trend indicates an average rupture speed of 1.5–2.0 km/s.

reproduce the moment tensor with a shallowly dipping nodal plane, which is robustly determined from the long-period seismic waves. Such a model would additionally produce coastal subsidence inconsistent with the observed uplift. Finally, a single planar fault cannot explain the non-double-couple fraction of the moment tensor. As a first step toward a more realistic fault model, we consider two planar faults (Figure 4). The first fault corresponds to the shallow dipping thrust fault required by the long-period seismological observations. The second is defined to match the Jordan Thrust and Kekerengu Fault, hereafter referred to simply as the Kekerengu Fault. We thus ignore the Papatea Fault and the discontinuous faulting in the southwest (mainshock epicentral region), for which we have only limited information, and which may have been contaminated by aftershocks. The strike of the Kekerengu Fault is set to 225°E and the dip angle to 50° (northwest), consistent with the average range of dips for the Jordan Thrust (28–48°) and the west (50–70°) and east (80–90°) Kekerengu Fault segments [see *Litchfield et al.*, 2014]. The Kekerengu Fault therefore appears to splay from the deeper shallowly dipping fault, hereafter called the main thrust fault, which also strikes 225°E and dips 25° to the northwest.

Our finite-fault model is derived from the inversion of 86 *P* wave and 47 SH wave waveforms (Figure S5). We crop the seismograms into segments of 125 s duration. The rupture is assumed to initiate at the USGS-NEIC hypocenter (42.757°S 173.077°E) with a hypocentral depth of 23 km, extending from 8 km to 38 km on the shallowly dipping fault, which extends offshore (E1 in Figure 4a). The initial rake angle is 100°, which can vary up to ±45° during the inversion. To reproduce the high rupture speed near the epicenter, as well as the overall low rupture speed, we set up 16 subfault source time functions with 3.0 s risetime triangles lagged by 3.0 s, for a total possible subfault duration of 51.0 s. For the dominant strike-slip behavior on the Kekerengu Fault, we constrain the rake angle to 175°, allowing for a small variation of ±20° in the inversion to reduce the trade-off with slip on the main thrust (due to the constraints of using only teleseismic data). The rupture on the Kekerengu Fault is assumed to extend from the surface to about 27 km with the initial rupture at 13.5 km (E2 in Figure 4b). The subfault source time function is parameterized with 16 1.5 s risetime triangles lagged by 1.5 s, for a total possible subfault duration of 25.5 s. We vary the parameters of the inversion, such as the constraints placed on rake and rupture velocity, and consistently find that the source model involved initial rupture with oblique slip motion on the main thrust fault. The moment rate stays relatively small for about 60 s and then rises abruptly during a ~20 s burst (Figure 3). This burst in the moment rate function is due to the simultaneous rupture along the main thrust fault and the Kekerengu Fault (Figure 3). According to this model, 60% of the total seismic moment was due to oblique slip on the main thrust with a centroid

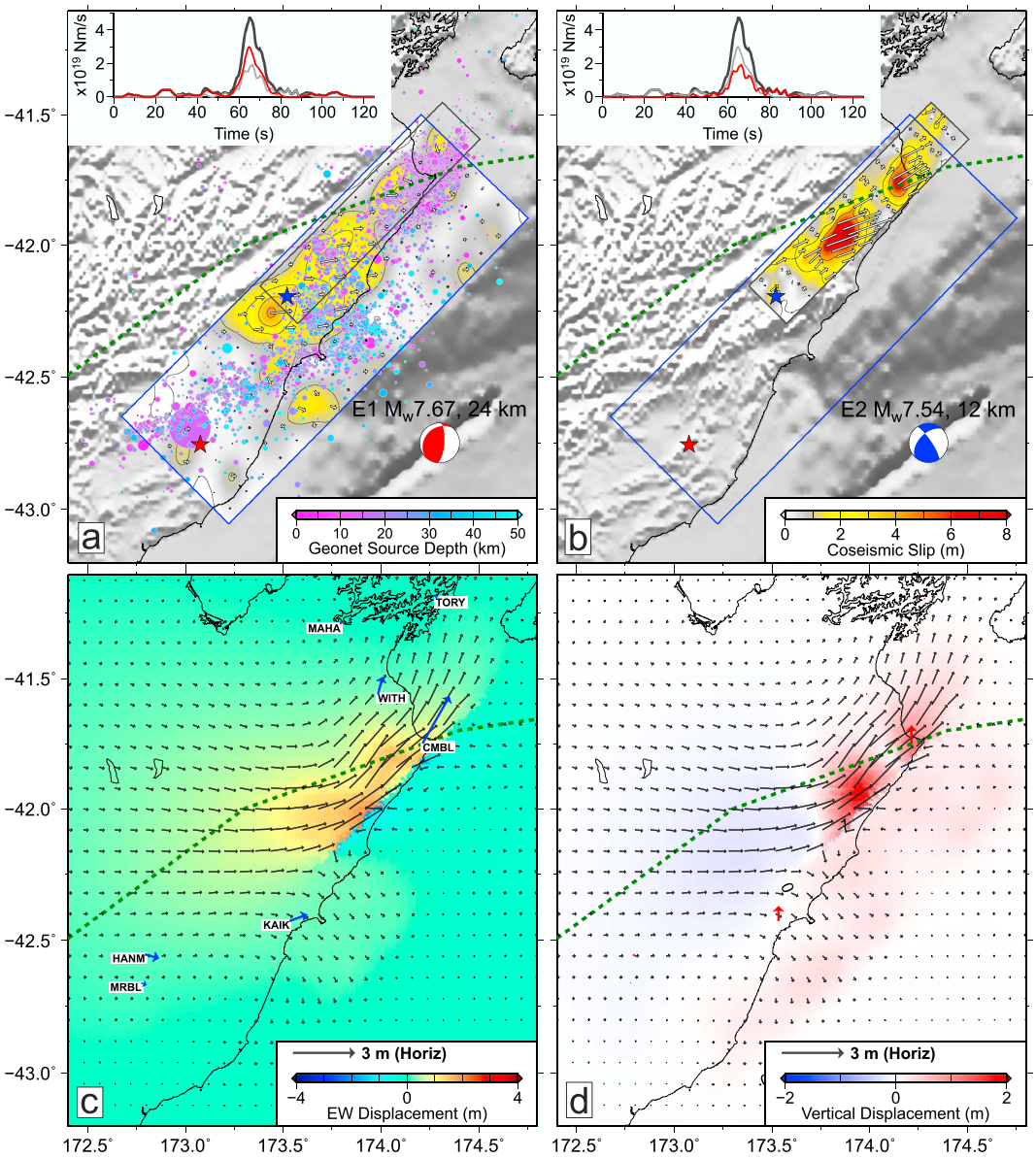

Figure 4. (a) Coseismic slip distribution on the fault E1 along with the corresponding moment tensor solution (red beach ball). The red and blue stars are the initiations for rupture on the faults E1 (same as USGS-NEIC epicenter) and E2, respectively. The circles colored for depth show aftershock and main shock epicenters from the GNS catalogue (http://info.geonet.org.nz/display/appdata/Earthquake+Catalogue). The inset shows the moment release rate as function of time from only source E1 (red), only E2 (black), and E1 + E2 (gray). (b) Coseismic slip distribution on fault E2 along with the corresponding moment tensor solution (blue beach ball). The inset shows the moment release rate as function of time from only source E2 (red), only E1 (black), and E1 + E2 (gray). Other symbols are same as Figure 4a. (c) The black vectors show horizontal surface displacements predicted by our slip model. The color coding shows amplitude of eastward component. The blue arrows show coseismic horizontal displacements produced by the Nevada Geodetic Laboratory (http://geodesy.unr.edu). (d) The vectors show horizontal surface displacements predicted by our source model. The color coding shows amplitude of vertical surface deformation.

depth of ~22 km, while the Kekerengu Fault accounts for the remaining 40% with a centroid depth of ~10 km. The exact slip portioning varies with imposed fault geometries, rupture initiation time, rupture expansion speed, and/or source time functions for each fault. It cannot be reliably determined from teleseismic data only, although our inversions show that substantial seismic energy is released from the main thrust. Our

model does not fit very well the early part of the seismograms (Figure S5) probably due to the simplified or inadequate fault geometry near the epicenter. Nevertheless, the large displacements between 60 s and 80 s after the onset of the rupture are well fit in both phase and amplitude. We explored various model parameters, such as fault dip angle, and found the simultaneous rupture of the Kekerengu Fault to be a robust feature of these inversions (we do not attempt to resolve small-scale details, which will require a more detailed analysis incorporating all available geodetic data in the inversion). The various inversions all imply dominantly strike-slip motion on the Kekerengu Fault with surface displacements consistent with those measured from correlation of Landsat8 satellite images (Figures 2 and 4c) and oblique slip on the main thrust giving overall uplift along the coastline.

4. Discussion-Conclusion

Surface deformation measured from correlation of optical satellite images clearly shows that the Kaikoura earthquake ruptured a steeply dipping fault with dominantly strike-slip motion. This fault cannot alone explain the relatively shallow dip angle and large thrust motion revealed by the long-period seismic waveforms. Clearly, the Kaikoura earthquake must have involved simultaneous rupture of the Kekerengu Fault and another fault with a substantial component of thrust motion. We calculate the equivalent moment tensor from our finite source model and found it to be remarkably consistent with the gCMT solution (Figure 1). Our model thus provides a satisfying explanation for the non-double-couple component of the moment tensor solution. Figure 4c shows the pattern of horizontal and vertical displacements predicted by our seismological source model. We note that the model predicts significant uplift in the offshore region of South Island. The region of uplift is consistent with the hanging wall region of the Kekerengu Bank Thrust Fault [*Barnes and Audru*, 1999], although we cannot confirm if this structure was activated during the main shock. This prediction is qualitatively consistent with a tsunami which affected the coastline following the main shock, producing 2.5 m wave heights recorded by the tsunami gauge at Kaikoura (https://www.geonet.org.nz/tsunami). Comparison with the GPS displacements determined by the University of Reno (Figure 4c) shows a qualitative agreement. The eastward displacements revealed by the GPS stations clearly require thrust motion in addition to the dominantly strike-slip motion on the Kekerengu Fault, which strongly affects the signal recorded at CMBL. We note that the patch of slip on the main thrust near the epicenter would need to be more compact and closer to station KAIK to better fit the displacement at this site (Figure 4). However, we also note that station KAIK is located close ($<$10 km) to the Hundalee Fault (Figures 2 and S2), and so may be influenced by surface slip on this structure. A more complex fault geometry is probably needed to fit the ground deformation in the epicentral area and the early part of the rupture. We leave to further investigations the determination of a refined source model from the joint inversion of static and dynamic (waveforms) and surface displacements. There is indeed no doubt that the source model can be refined significantly, thanks in particular to interferometric synthetic aperture radar measurements of surface deformation that have been produced by various groups (e.g., GNS Science, comet.nerc.ac.uk, aria.jpl.nasa.gov, and eorc.jaxa.jp), coupled with correlation of high-resolution stereo optical satellite imagery, detailed field measurements, high-rate GPS records, and strong motion data that were recorded during this event (info.geonet.org.nz/display/appdata/Strong-Motion+Data).

The 2016 Kaikoura main shock broke a previously undocumented thrust fault underlying the Marlborough coastline, in addition to the previously unmapped Papatea Fault, and several other less well-known structures (e.g., Hundalee Fault and Humps Fault Zone). The main thrust fault could be the southwest extension of the Hikurangi Megathrust [e.g., *Wallace et al.*, 2009] or some other thrust fault within the fore-arc wedge. Active NW-dipping thrust faults have been well-documented in the offshore region between Kaikoura and Blenheim from seismic reflection data [e.g., *Barnes and Audru*, 1999]. The down-dip projection of offshore thrust faults to the northwest, beneath the Marlborough region, is also consistent with a sequence of uplifted Quaternary shorelines preserved along the coastline [*Ota et al.*, 1996]. These faults as well as the Kekerengu and Jordan faults might thus be seen as splaying from some underlying thrust fault, possibly interpreted as the southern extension of the Hikurangi Megathrust. Splay faults are commonly observed at converging plate boundaries and are suspected to pose a seismic and tsunamic hazard [e.g., *Park et al.*, 2002]. Coseismic activation of splay faults has been suspected in past megathrust earthquakes based on observed surface deformation [e.g., *Plafker*, 1965] or tsunamis [e.g., *Baba et al.*, 2006]. However, the Kaikoura earthquake is the first time where the contribution of slip on a splay fault is clearly isolated in the seismological waveforms. An alternative

interpretation is that the Marlborough Faults would be "listric" with their dip angle decreasing with depth and that the strike slip and oblique thrusting would have occurred on two disconnected faults. Future studies will be required to better resolve the subsurface geometry of faults in the region and their connection with the western termination of the Hikurangi Megathrust.

This event follows other recent large earthquakes in New Zealand, such as the 2010–2011 Canterbury earthquake sequence [*Elliott et al.*, 2012], which also broke previously unmapped active faults. A recent statistical analysis of historical earthquakes in New Zealand [*Nicol et al.*, 2016] indicates about half of all large historical earthquakes ($M_w > 7.0$) ruptured faults that would not have been identified as active prior to the event (based on today's state of knowledge). Therefore, when considering the seismic hazard of the Marlborough region, and the influence of the Kaikoura earthquake on the state of stress of neighboring fault systems (e.g., the Hope, Awatere, Clarence, and Wairu Faults), consideration should also be given to potentially unknown faults (e.g., blind thrust faults), in both the onshore and offshore region, which is generally less-well mapped, and may feature tsunamigenic faults.

We conclude that simultaneous strike-slip motion on the Kekerengu Fault and oblique slip on a deeper fault with shallow dip angle, from which the Kekerengu Fault seems to splay, is in any case a robust feature of the available seismic and optical satellite data.

Acknowledgments

Landsat8 satellite imagery was obtained from the USGS (earthexplorer.usgs.gov/). Seismic data were obtained from the Australian seismic network. Financial support is acknowledged from SCEC (L.Y. and J.P.A.), CNRS, and ISTerre (J.H.). We thank Francois Ayoub, Zacharie Duputel, Romain Jolivet, and James Dolan for helpful discussions. Various images in this paper were created by using the Generic Mapping Tools (GMT) software [*Wessel and Smith*, 1998].

References

Avouac, J. P., F. Ayoub, S. Wei, J. P. Ampuero, L. Meng, S. Leprince, R. Jolivet, Z. Duputel, and D. Helmberger (2014), The 2013, M_w 7.7 Balochistan earthquake, energetic strike-slip reactivation of a thrust fault, *Earth Planet. Sci. Lett.*, *391*, 128–134.

Avouac, J.-P., and S. Leprince (2015), Geodetic imaging using optical systems, in *Treatise on Geophysics*, edited by G. Schubert, pp. 387–424, Elsevier, Oxford.

Ayoub, F., L. Leprince, and J.-P. Avouac (2015), User's guide to COSI-CORR: Co-registration of optically sensed images and correlation, California Institute of Technology. [Available at http://www.tectonics.caltech.edu/slip_history/spot_coseis/pdf_files/CosiCorr-Guide2015a.pdf.]

Baba, T., P. R. Cummins, T. Hori, and Y. Kaneda (2006), High precision slip distribution of the 1944 Tonankai earthquake inferred from tsunami waveforms: Possible slip on a splay fault, *Tectonophysics*, *426*(1–2), 119–134.

Barnes, P. M., and J.-C. Audru (1999), Recognition of active strike-slip faulting from high-resolution marine seismic reflection profiles: Eastern Marlborough Fault System, New Zealand, *Geol. Soc. Am. Bull.*, *111*(4), 538–559.

Bormann, P., M. Baumbach, G. Bock, H. Grosser, G. L. Choy, and J. Boatwright (2009), Seismic sources and source parameters, in *New Manual of Seismological Observatory Practice (NMSOP)*, edited by P. Bormann, pp. 1–94, Potsdam, Deutsches GeoForschungsZentrum GFZ.

Copley, A., J.-P. Avouac, J. Hollingsworth, and S. Leprince (2011), The 2001 M_w 7.6 Bhuj earthquake, low fault friction, and the crustal support of plate driving forces in India, *J. Geophys. Res.*, *116*, B08405, doi:10.1029/2010JB008137.

Elliott, J. R., E. K. Nissen, P. C. England, J. A. Jackson, S. Lamb, Z. Li, M. Oehlers, and B. Parsons (2012), Slip in the 2010–2011 Canterbury earthquakes, New Zealand, *J. Geophys. Res.*, *117*, B03401, doi:10.1029/2011JB008868.

Hartzell, S. H., and T. H. Heaton (1983), Inversion of strong ground motion and teleseismic waveform data for the fault rupture history of the 1979 Imperial Valley, California, earthquake, *Bull. Seismol. Soc. Am.*, *73*(6A), 1553–1583.

Hollingsworth, J., S. Leprince, F. Ayoub, and J.-P. Avouac (2012), Deformation during the 1975–1984 Krafla rifting crisis, NE Iceland, measured from historical optical imagery, *J. Geophys. Res.*, *117*, B11407, doi:10.1029/2012JB009140.

Ishii, M., P. M. Shearer, H. Houston, and J. E. Vidale (2005), Extent, duration and speed of the 2004 Sumatra-Andaman earthquake imaged by the Hi-Net array, *Nature*, *435*(7044), 933–936.

Knuepfer, P. L. K. (1992), Temporal variations in latest Quaternary slip across the Australian-Pacific Plate Boundary, northeastern South Island, New Zealand, *Tectonics*, *11*, 449–464, doi:10.1029/91TC02890.

Leprince, S., S. Barbot, F. Ayoub, and J.-P. Avouac (2007), Automatic and precise orthorectification, coregistration, and subpixel correlation of satellite images, application to ground deformation measurements, *IEEE Trans. Geosci. Remote Sens.*, *45*(6), 1529–1558.

Litchfield, N. J., et al. (2014), A model of active faulting in New Zealand, *New Zealand, J. Geol. Gephys.*, *57*, 32–56, doi:10.1080/00288306.2013.854256.

Litchfield, N. J., et al. (2016), 14th November 2016 Kaikoura earthquake. Preliminary earthquake geology observations, *GNS Sci.*, doi:10.21420/G2MW2D.

Mason, D. P. M., and T. A. Little (2006), Refined slip distribution and moment magnitude of the 1848 Marlborough earthquake, Awatere Fault, New Zealand, *New Zealand J. Geol. Geophys.*, *49*(3), 375–382.

Nicol, A., R. Van Dissen, M. W. Stirling, and M. C. Gerstenberger (2016), Completeness of the paleoseismic active-fault record in New Zealand, *Seismol. Res. Lett.*, doi:10.1785/0220160088.

Ota, Y., B. Pillans, K. Berryman, A. Beu, T. Fujimori, T. Miyauchi, G. Berger, A. G. Beu, and F. M. Climo (1996), Pleistocene coastal terraces of Kaikoura Peninsula and the Marlborough coast, South Island, New Zealand, *New Zealand J. Geol. Geophys.*, *39*(1), 51–73.

Park, J. O., T. Tsuru, S. Kodaira, P. R. Cummins, and Y. Kaneda (2002), Splay Fault branching along the Nankai Subduction Zone, *Science*, *297*(5584), 1157–1160.

Plafker, G. (1965), Tectonic deformation associated with the 1964 Alaskan earthquake, *Science*, *148*, 1675–1687.

Van Dissen, R., and R. S. Yeats (1991), Hope Fault, Jordan Thrust, and uplift of the seaward Kaikoura Range, New Zealand, *Geology*, *19*(4), 393–396.

Wallace, L. M., et al. (2009), Characterizing the seismogenic zone of a major plate boundary subduction thrust: Hikurangi Margin, New Zealand, *Geochem. Geophys. Geosyst.*, *10*, Q10006, doi:10.1029/2009GC002610.

Wessel, P., and W. H. F. Smith (1998), New, improved version of Generic Mapping Tools released, *Eos Trans. AGU*, *79*(47), 579, doi:10.1029/98EO00426.

Xu, Y., K. D. Koper, O. Sufri, L. Zhu, and A. R. Hutko (2009), Rupture imaging of the M_w 7.9 12 May 2008 Wenchuan earthquake from back projection of teleseismic *P* waves, *Geochem. Geophys. Geosyst.*, *10*, Q04006, doi:10.1029/2008GC002335.

Ye, L., T. Lay, H. Kanamori, and L. Rivera (2016), Rupture characteristics of major and great ($M_w \geq 7.0$) megathrust earthquakes from 1990 to 2015: 1. Source parameter scaling relationships, *J. Geophys. Res. Solid Earth*, *121*, 826–844, doi:10.1002/2015JB012426.

Zinke, R., J. Hollingsworth, and J. F. Dolan (2014), Surface slip and off-fault deformation patterns in the 2013 M_w 7.7 Balochistan, Pakistan earthquake: Implications for controls on the distribution of near-surface co-seismic slip, *Geochem. Geophys. Geosyst.*, *15*, 5034–5050, doi:10.1002/2014GC005538.